ACS OMEGA

http://pubs.acs.org/journal/acsodf
Article

Theoretical Investigation of a New Physical Method for Fat Removal by Melting: A Case Study of Caprate Triglyceride

Peilin Li, Yining Li, Yawen Li, Jingyu Zhang, Zhengfei Wen, and Peng Zhang*

Cite This: ACS Omega 2025, 10, 11354−11358
Read Online
ACCESS | Metrics & More | Article Recommendations | Supporting Information

ABSTRACT: Obesity is the most common unhealthy characteristic; it not only makes people feel troubled about their appearance but also causes many diseases that threaten people's health and lives. Liposuction is a widely promoted plastic surgery technique for removing excess fat from people with obesity. Typically, liposuction involves the application of vibration to break fat cells and, thus, can cause harm to the body. This paper describes a theoretical proposal for the use of a selected-frequency terahertz laser as a new physical approach for quickly removing fat by melting. Tricaprin, a medium-chain triglyceride, was examined in a case study that involved first-principles density functional theory calculations, together with infrared absorption and Raman scattering experiments. The vibrational mode of the highest infrared absorption peak of tricaprin (1763 cm^{-1} (simulation), 1735 cm^{-1} (experiment)) was found to represent a carbonyl group (C═O) stretching vibration. Due to the high electronegativity of oxygen, this C═O bond is strongly correlated with intermolecular hydrogen bonding. Thus, it efficiently absorbs energy, enabling a rapid breakdown of the solid structure of tricaprin. This process could potentially be applied as a weight-loss treatment, as tricaprin is present in triglycerides, which are the typical component of fat. In addition, this process could be used in medical physics applications such as for the treatment of arteriosclerosis.

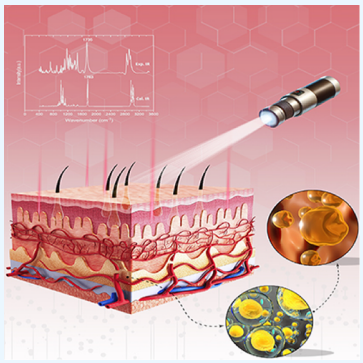

INTRODUCTION

In recent years, the issue of obesity has emerged as a significant focus in the field of public health.[1] The rising prevalence of obesity is associated with various aspects of modern living, such as suboptimal dietary choices, limited physical activity, and high levels of occupational stress. Obesity is also related to a multitude of chronic diseases.[2−5] Currently, a variety of approaches are implemented to manage obesity, such as dietary modifications, the use of weight-loss medications, control of fluid intake, and participation in exercise regimens. However, when these methods are overly utilized in the pursuit of body weight management, they may potentially have adverse effects and may not yield the desired outcomes. For instance, extreme dietary restrictions and rapid weight reduction can lead to a decline in the basal metabolic rate, thereby slowing energy expenditure. As a result, weight loss progress may be hampered and weight regain could be facilitated.[6] Repeated fluctuations in body weight, known as weight cycling, are associated with an increased risk of CVD and all-cause mortality and may also give rise to health issues like inflammation, insulin resistance, and elevated blood pressure.[7] Additionally, rapid or unnecessary weight loss might lead to a reduction in lean body mass, particularly skeletal muscle mass, which could significantly impact physical function and long-term health, especially among the elderly and athletes.[8]

Infrared (IR) radiation is categorized into three bands, namely near-IR (0.78−3.00 μm), mid-IR (3.00−50.00 μm), and far-IR (50.00−1000.00 μm) bands.[9] In recent years, IR light therapy has gained widespread attention in the medical and beauty fields.[10−16] In particular, IR light therapy has been used to induce beige fat activation via the heat shock factor 1−heterogeneous nuclear ribonucleoproteins A2/B1 transcriptional axis to alleviate obesity,[10] indicating its utility for aiding weight loss. It has also been used to treat gingival incisions,[17] soft tissue injuries,[18] skin ulcers,[19] carpal tunnel syndrome,[20] and oral mucositis[21] and to support wound healing[22] and nerve repair.[23−25] In IR light therapy, photon absorption by molecules in living cells and tissues triggers various signaling pathways, leading to energy conversion. Consequently, certain molecules are photoexcited to electronically excited states, which alter these molecules' conformation and function, resulting in the activation of signaling pathways that mediate cellular metabolism.[11]

Chung et al. noted that although low-level laser therapy is now used to treat a wide variety of ailments, its numerous parameters (such as wavelength, fluence, power density, pulse structure, and timing of applied light) must be carefully considered for each treatment.[26] In the current study, we focused on the selection of the laser wavelength in IR light therapy from a physical perspective to devise an innovative fat-

Received: December 12, 2024
Revised: February 4, 2025
Accepted: February 20, 2025
Published: February 26, 2025

https://doi.org/10.1021/acsomega.4c11242
ACS Omega 2025, 10, 11354−11358

melting method. The main components of fat are triglycerides, and caprate triglyceride (tricaprin), a representative medium-chain triglyceride, is useful for studying the interaction between fat molecules and IR light. Accordingly, we conducted a comprehensive investigation to determine which bond vibrations of tricaprin were responsible for the high-intensity absorption peaks in its IR spectrum. Based on the efficient photon−phonon resonance absorption (PPRA), the special IR wavelength radiation will lead to rapid fat melting and achieve the goal of fat reduction.

METHODS

Tricaprin was purchased from Meryer Chemical Technology Co., Ltd. (Shanghai, China). Raman spectroscopy (inVia plus, Renishaw) was conducted at room temperature using a 532 nm laser in the 50−4000 cm^{-1} range and at a resolution of 0.7 cm^{-1}. IR spectroscopy (VERTEX 70v, Bruker) was conducted at room temperature in the 400−4000 cm^{-1} range and at a resolution of 0.15 cm^{-1}.

As solid tricaprin is amorphous, mimicking its intermolecular interactions would require construction of a huge supercell. On the other hand, the IR and Raman spectra of tricaprin contained no characteristic peaks in hydrogen-bonding regions. Thus, calculations were performed for a single molecule of tricaprin to determine its intramolecular vibrational modes. The first-principles density functional theory (DFT) DMol^3 code was used to perform geometry optimization of tricaprin and simulate its vibrational spectra.[27] The Becke−Lee−Yang−Parr (BLYP) exchange-correlation functional of the generalized gradient approximation was the best matchable functional for calculating the vibrational spectra. The self-consistent field convergence criterion was set to 1×10^{-9} eV/atom to ensure structural stability. The energy convergence was set to 1×10^{-7} eV/atom. The basis set was DNP with the DSPP pseudopotential, and the energy cutoff was 3.7 Å. Based on the harmonic approximation, all of the vibrational normal modes were calculated. Comparison with the experimental data enabled the key peaks to be assigned by the analysis of the dynamic process of each vibrational mode.

RESULTS AND DISCUSSION

Tricaprin comprises a glycerol backbone and three capric-acid-derived side chains. It lacks symmetry and belongs to the C_1 point group. A saturated monoacid glyceride has the approximate formula $C_{3+3n}H_{2+6n}O_6$, where $(n - 1)$ is the number of carbon atoms in the alkyl chain of the fatty acid.[28] As $n = 10$ in tricaprin, its molecular formula is $C_{33}H_{62}O_6$, indicating that it consists of 101 atoms. Thus, its number of vibrational modes is $3 \times 101 - 3 = 300$. All of these vibrational modes may couple with photons, which can be detected via IR and Raman spectroscopy. However, the intensities of each peak in the IR and Raman spectra may vary with the selection rules. Thus, we focused on the characteristic IR peaks that exhibited a high PPRA and examined the use of Raman peaks for verification.

Figure 1 shows a simulated Raman spectrum and the experimental Raman spectrum of tricaprin. In the simulated Raman spectrum, the strongest peak was at 2982 cm^{-1}, followed by one peak at 3043 cm^{-1}. These peaks were caused by C−H vibrations. In contrast, the experimental Raman spectrum contained strong peaks at 2872, 2883, 2935, and 2964 cm^{-1} in this band. Compared with the peaks in the experimental Raman spectrum, those in the simulated Raman spectrum were slightly blue-shifted because the former was obtained from a sample of tricaprin, while the latter was generated from a single-molecule model of tricaprin. The multiple peaks in the experimental Raman spectrum were due to a decreased intramolecular bond strength, resulting from intermolecular interactions in the tricaprin sample. The high intensities of the peaks around 3000 cm^{-1} in the simulated Raman spectrum meant that other peaks in this area were too small to be visible. However, the peaks in the simulated Raman spectrum are in good agreement with those in the experimental Raman spectrum. For example, the five peaks in the region from 800 to 1600 cm^{-1} were at 890, 1061, 1124, 1298, and 1441 cm^{-1} in the experimental Raman spectrum and at 896, 1016, 1111, 1285, and 1474 cm^{-1} in the simulated Raman spectrum.

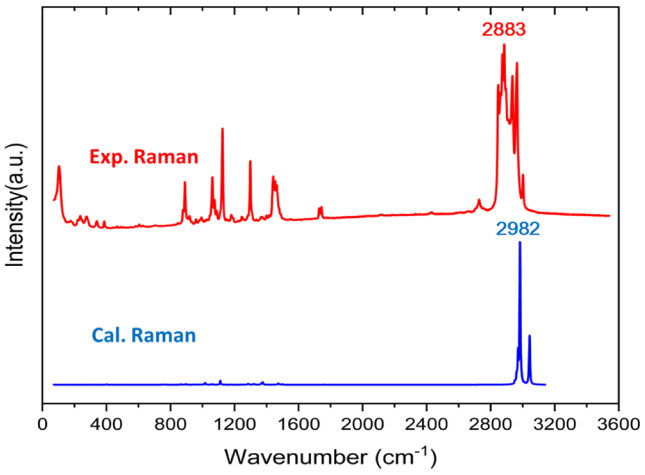

Figure 1. Experimental Raman spectrum (red line) and simulated Raman spectrum (blue line) of tricaprin. The wavenumber of the strongest peak in each spectrum is indicated.

Figure 2 presents the simulated IR spectrum and the experimental IR spectrum of tricaprin. The most intense peak appeared at 1763 cm^{-1} in the simulated IR spectrum and at 1737 cm^{-1} in the experimental IR spectrum. In addition, there were peaks at approximately 3000 cm^{-1}, representing rather

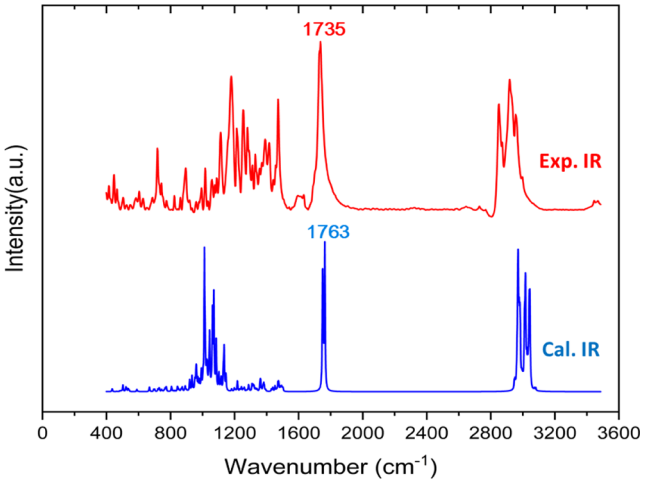

Figure 2. Experimental IR spectrum (red line) and simulated IR spectrum (blue line) of tricaprin. The wavenumber of the strongest peak in each spectrum is indicated.

https://doi.org/10.1021/acsomega.4c11242
ACS Omega 2025, 10, 11354−11358

strong C−H vibrations. However, the two spectra differed in the fingerprint region, i.e., at less than 1600 cm^{-1}. Specifically, many sharp peaks in the experimental IR spectrum were almost absent from the simulated IR spectrum. This mirrored the trend in the Raman spectra and indicates that the IR fingerprint region spectroscopic pattern of tricaprin is also affected by its molecular environment. Thus, as the simulated IR spectrum of tricaprin was generated from a single-molecule model, while the experimental IR spectrum was obtained from a sample of tricaprin, their respective fingerprint regions showed marked differences.

Based on an analysis of the dynamic process of the vibrational modes, we assigned them to skeletal vibrations, C−H bending vibrations, or stretching vibrations. We selected some relatively high-intensity characteristic peaks from 300 normal vibrational modes and compared them with experimental data, as shown in Table 1. The vibrational modes at less than 600 cm^{-1} were assigned to molecular skeletal vibrations. Two examples of such modes at 502 and 535 cm^{-1} are shown in Figure 3. The vibrations in this region involve complex motions along carbon chains. The vibrational modes at 600−1600 cm^{-1} were assigned to C−H bending vibrations, for simplicity. Two examples of such modes at 1070 and 1110 cm^{-1} are shown in Figure 3. Previous studies have assigned some peaks at 600−1600 cm^{-1} in Raman and IR spectra of lipids to fine vibrational modes. For example, Meksiarun et al. assigned IR peaks at 1121, 1080, 1068, 892, and 865 cm^{-1} to C−C bending vibrations of a lipid skeleton.[28] Bresson et al. assigned a strong peak at 1061 cm^{-1} and two weak peaks at 1177 and 1183 cm^{-1} in the Raman spectra of lipids of various carbon-chain lengths (n = 2, 11, 12, 14, and 16) to C−C skeletal vibrations. In addition, they assigned peaks at 890, 908, 920, 1086, 1100, and 1129 cm^{-1} in these spectra to asymmetric C−O−C vibrations.[29]

Bresson et al. also noted that three different motions between 1700 and 1780 cm^{-1} were C═O stretching vibrations.[29] In our study, two weak peaks were detected in the experimental Raman spectrum. The corresponding calculated vibrational modes were 1749, 1753, and 1763 cm^{-1}. Figure 4 shows these three kinds of C═O stretching vibrations, which are part of the "knot" group, and a C−H stretching vibration.

The above-described studies have shown that the spectra of various monoacid triglycerides exhibit similar variations as their carbon-chain lengths change. Moreover, O'Connor et al. analyzed the IR spectra of mono-, di-, and triglycerides[30] and found that they contained six prominent bands, which they posited had a common origin. They divided the spectra into the following six parts to make assignments: peaks at 3.30−3.37 μm (3030−2967 cm^{-1}) were assigned to C−H stretching vibrations; peaks at 5.71−5.77 μm (1751−1733 cm^{-1}) were assigned to C═O stretching vibrations; peaks at 6.83−6.88 μm (1464−1453 cm^{-1}) were assigned to C−H bending vibrations (doubly degenerate deformation of CH_3 and symmetrical deformation of CH_2); peaks at 7.23−7.35 μm (1383−1360 cm^{-1}) were assigned to C−H bending vibrations (symmetrical deformation of CH_3); peaks at 7.93−8.00 μm (1261−1250 cm^{-1}) were assigned to C−H in-plane wagging vibrations or CH_2 rocking vibrations; and peaks at 8.48−8.58 μm (1179−1165 cm^{-1}) were assigned to C−O stretching vibrations. The current study was focused on identifying the IR peaks of tricaprin with the highest absorption efficiency. Thus, the above-mentioned vibrational modes were not comprehensively examined. They key point was that irrespective of the length of the carbon chain of a triglyceride, the peaks representing C═O stretching vibrations are in a narrow band located at 1751−1733 cm^{-1}.

As shown in Figure 4, three kinds of vibrational modes for the C═O bond were identified in the IR spectra of tricaprin at 1749, 1753, and 1763 cm^{-1}, respectively. This energy splitting was due to the bond length and angle of the O−C═O structures varying between different positions. The most intense absorption peak in the simulated IR spectrum was at 1763 cm^{-1}, corresponding to the peak in the experimental IR spectrum at 1735 cm^{-1}. Examining the original experimental data revealed that the IR photon−phonon absorption rate for this peak was up to 42%. Thus, as shown in Figure 2, this is the best peak to target for PPRA. That is, if the frequency of a terahertz laser matched this peak, then an optimal photothermal effect would be realized. Moreover, the high electronegativity of C═O suggests that these groups in a given tricaprin molecule are involved in hydrogen bonding with neighboring tricaprin molecules. The resulting intermo-

Table 1. Calculated Normal Vibrational Modes, Corresponding Experimental IR and Raman Data, and Assigned Vibrations of Tricaprin

normal mode (cm^{-1})	exp. IR (cm^{-1})	exp. Raman (cm^{-1})	assigned vibration
435	433		skeletal deformation
502	503		skeletal deformation
520	524		skeletal deformation
535	538		skeletal deformation
589	582		skeletal deformation
896		890	C−H bending
919	920		C−H bending
933	933		C−H bending
959	958		C−H bending
992	993		C−H bending
1010	1016		C−H bending
1016		1061	C−H bending
1027	1033		C−H bending
1043			C−H bending
1061	1056		C−H bending
1070	1076		C−H bending
1084	1087		C−H bending
1111		1124	C−H bending
1134			C−H bending
1285		1298	C−H bending
1474		1465	C−H bending
1749			C═O stretching
1753			C═O stretching
1763	1735		C═O stretching
2970	2850		C−H stretching
2977	2870		C−H stretching
2981	2918		C−H stretching
2982		2883	C−H stretching
3017	2954		C−H stretching
3024	2997		C−H stretching
3029			C−H stretching
3043		3001	C−H stretching

https://doi.org/10.1021/acsomega.4c11242
ACS Omega 2025, 10, 11354−11358

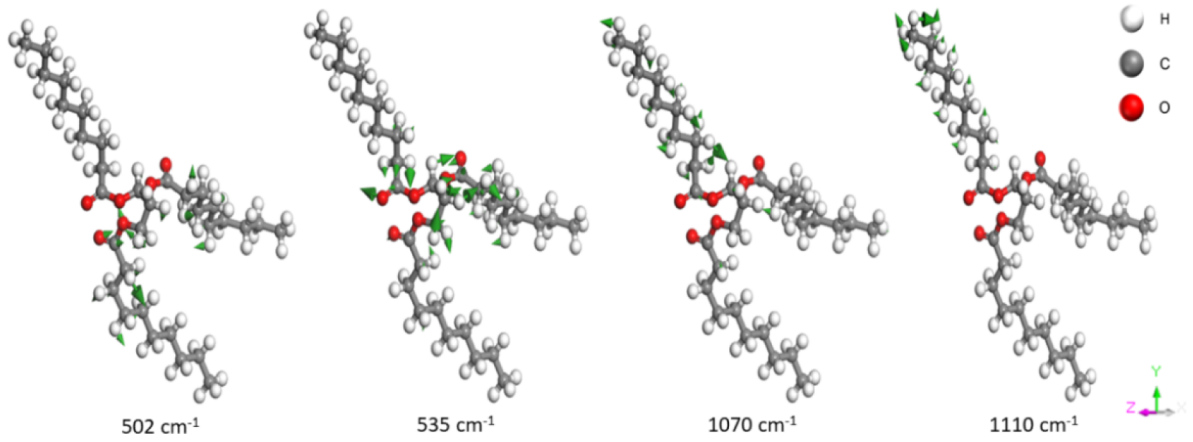

Figure 3. Examples of the four vibrational modes of tricaprin. The first two (from the left) show complex skeletal vibrations, and the last two show H−C−H or C−C−H bending vibrations. The green arrow indicates the direction and magnitude of motion.

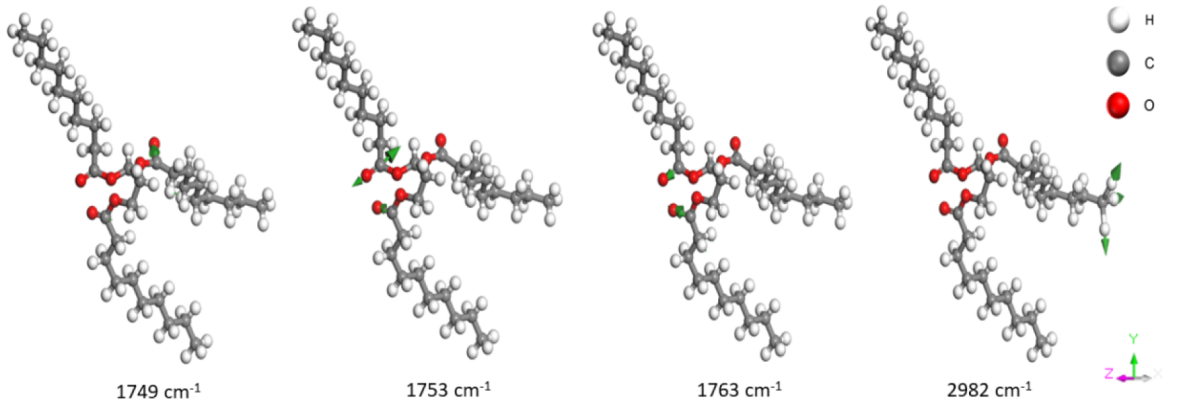

Figure 4. Four examples of vibrational modes. The first three structures (from the left) show C═O stretching modes, and the last structure shows a C−H stretching mode. The green arrow represents the direction and magnitude of the motion.

lecular hydrogen bond network would make a major contribution to the solid structure of tricaprin. Thus, solid tricaprin may be efficient to break its intermolecular hydrogen bonds through PPRA and thus cause it to rapidly liquefy. Further experiments will be performed to explore this intriguing possibility.

CONCLUSIONS

In this study, we performed DFT simulations and IR and Raman spectroscopy to examine the structural properties of tricaprin, a typical medium-chain triglyceride. The 300 calculated vibrational modes of tricaprin were assigned to four types of vibrations in corresponding energy bands: skeletal vibrations, C−H bending vibrations, C═O stretching vibrations, and C−H stretching vibrations. It was found that in the lowest frequency energy band (<600 cm^{-1}), many atoms of tricaprin participate in collective motion that results in skeletal deformations. In the midenergy band (600−1600 cm^{-1}), there are many kinds of dihedral angle deformations, i.e., C−H bending vibrations. In the high, narrow band (1700−1800 cm^{-1}), there are C═O stretching vibrations. In the highest energy band (2800−3100 cm^{-1}), there are C−H stretching vibrations.

Compared with previous studies, the above-mentioned assignments are less certain. However, it was confirmed that the most efficient IR absorption peak is exhibited by C═O (which has vibrational modes at 1749, 1753, and 1763 cm^{-1}). This peak was present at 1735 cm^{-1} (52 THz) in the experimental IR spectrum and was found to have an IR photon−phonon absorption rate of 42%. Moreover, this vibrational frequency is rather stable across various triglycerides, irrespective of the length of their carbon chains. Thus, we postulate that this peak can also be detected in the IR spectra of other solid triglycerides, which are the main components of fat. Therefore, we propose that by using selected frequency laser radiation on fat cells in the human body, a fast-melting phase transition may be achieved. In this regard, a 52-THz high-power laser would likely be optimal, as it would result in efficient PPRA by C═O in triglycerides. In future work, we will explore this novel technique in experimental tests.

Despite the theoretical prospect, translating these findings into practical applications faces challenges. The single-molecule model used in the calculations may not fully represent the complexity of real fat tissue. Precise control of the laser parameters in vivo is difficult. Experimental validation is crucial to confirm the effectiveness and safety, including potential side effects such as tissue damage and immune responses. Long-term effects of repeated treatments also require further study.

ASSOCIATED CONTENT

Supporting Information

The Supporting Information is available free of charge at https://pubs.acs.org/doi/10.1021/acsomega.4c11242.

https://doi.org/10.1021/acsomega.4c11242
ACS Omega 2025, 10, 11354−11358

Molecule structure of tricaprin (PDF)

AUTHOR INFORMATION

Corresponding Author

Peng Zhang − *Shandong Provincial Key Laboratory of Nuclear Science, Nuclear Energy Technology and Comprehensive Utilization, Weihai Frontier Innovation Institute of Nuclear Technology, Shandong University, Weihai 264209, China;* orcid.org/0000-0002-1099-6310; Email: zhangpeng@sdu.edu.cn

Authors

Peilin Li − *Shandong Provincial Key Laboratory of Nuclear Science, Nuclear Energy Technology and Comprehensive Utilization, Weihai Frontier Innovation Institute of Nuclear Technology and School of Space Science and Technology, Shandong University, Weihai 264209, China; SDU-ANU Joint Science College, Shandong University, Weihai 264209, China*

Yining Li − *School of Space Science and Technology, Shandong University, Weihai 264209, China*

Yawen Li − *School of Space Science and Technology, Shandong University, Weihai 264209, China*

Jingyu Zhang − *School of Space Science and Technology, Shandong University, Weihai 264209, China*

Zhengfei Wen − *School of Space Science and Technology, Shandong University, Weihai 264209, China*

Complete contact information is available at: https://pubs.acs.org/10.1021/acsomega.4c11242

Notes

The authors declare no competing financial interest.

ACKNOWLEDGMENTS

We are grateful to the project ZR2022MA017 supported by the Shandong Provincial Natural Science Foundation for financial support. The numerical calculations were performed on the supercomputing system at the Supercomputing Center, Shandong University, Weihai.

REFERENCES

(1) James, W. P. T. Obesity: A Global Public Health Challenge. *Clin. Chem.* **2018**, *64*, 24−29.

(2) Lindstrom, M.; Isacsson, S.; Merlo, J. Increasing prevalence of overweight, obesity and physical inactivity: two population-based studies 1986 and 1994. *Eur. J. Public Health* **2003**, *13*, 306−312.

(3) Mokdad, A. H.; Ford, E. S.; Bowman, B. A.; Dietz, W. H.; Vinicor, F.; Bales, V. S. Prevalence of obesity, diabetes, and obesity-related health risk factors, 2001. *JAMA* **2003**, *289*, 76−79.

(4) Dwivedi, A. K.; Dubey, P.; Cistola, D. P.; Reddy, S. Y. Association between Obesity and Cardiovascular Outcomes: Updated Evidence from Meta-analysis Studies. *Curr. Cardiol. Rep.* **2020**, *22* (4), 25.

(5) Jepsen, S.; Suvan, J.; Deschner, J. The association of periodontal diseases with metabolic syndrome and obesity. *Periodontology 2000* **2020**, *83*, 125−153.

(6) Brownell, K. D.; Rodin, J. The dieting maelstrom: Is it possible and advisable to lose weight? *Am. Psychol.* **1994**, *49* (9), 781−791.

(7) Ashtary-Larky, D.; Bagheri, R.; Abbasnezhad, A.; Tinsley, G. M.; Alipour, M.; Wong, A. Effects of gradual weight loss v. rapid weight loss on body composition and RMR: a systematic review and meta-analysis. *Br. J. Nutr.* **2020**, *124*, 1121−1132.

(8) McCarthy, D.; Berg, A. Weight Loss Strategies and the Risk of Skeletal Muscle Mass Loss. *Nutrients* **2021**, *13* (7), 2473.

(9) Vatansever, F.; Hamblin, M. R. Far infrared radiation (FIR): Its biological effects and medical applications: Ferne Infrarotstrahlung: Biologische Effekte und medizinische Anwendungen. *Photonics Lasers Med.* **2012**, *1* (4), 255−266.

(10) Li, Y.; Wang, D.; Ping, X.; et al. Local hyperthermia therapy induces of white fat and treats. *Cell* **2022**, *185*, 949−966.

(11) Zhu, Q.; Xiao, S.; Hua, Z.; Yang, D.; Hu, M.; Zhu, Y. T.; Zhong, H. Near Infrared (NIR) Light Therapy of Eye Diseases: A Review. *Int. J. Med. Sci.* **2021**, *18*, 109−119.

(12) Tsai, S. R.; Hamblin, M. R. Biological effects and medical applications of infrared radiation. *J. Photochem. Photobiol., B* **2017**, *170*, 197−207.

(13) Sun, H.; Zhang, Q.; Li, J.; Peng, S.; Wang, X.; Cai, R. Near-infrared photoactivated nanomedicines for photothermal synergistic cancer therapy. *Nano Today* **2021**, *37*, 101073.

(14) Johnstone, D. M.; Moro, C.; Stone, J.; Benabid, A.-L.; Mitrofanis, J. Turning On Lights to Stop Neurodegeneration: The Potential of Near Infrared Light Therapy in Alzheimer's and Parkinson's Disease. *Front. Neurosci.* **2016**, *9*, 500.

(15) Cristiano, L. Use of infrared as a complementary treatment approach in medicine and aesthetic medicine. *Asp. J. Biomed. Clin. Case Rep.* **2019**, *29* (2), 77−81.

(16) Pang, X.-F.; Deng, B.; Xiao, H.-L.; Cai, G.-P. The Investigation of Property of Radiation and Absorbed of Infrared Lights of the Biological Tissues. *J. Infrared, Millimeter, Terahertz Waves* **2010**, *31*, 521−532.

(17) Madi, M.; Mahmoud, M. M. The evaluation of healing effect of low-level laser treatment following gingivectomy. *Beni-Suef Univ. J. Basic Appl. Sci.* **2020**, *9* (1), 25.

(18) Han, D.; Xu, J.; Wang, Z.; Yang, N.; Li, X.; Qian, Y.; Li, G.; Dai, R.; Xu, S. Penetrating effect of high-intensity infrared laser pulses through body tissue. *RSC Adv.* **2018**, *8*, 32344−32357.

(19) Horton, L.; Brady, J.; Kincaid, C. M.; Torres, A. E.; Lim, H. W. The effects of infrared radiation on the human skin. *Photodermatol., Photoimmunol. Photomed.* **2023**, *39* (6), 549−555.

(20) Irvine, J.; Chong, S.; Amirjani, N.; Chan, K. Double-blind randomized controlled trial of low-level laser therapy in carpal tunnel syndrome. *Muscle Nerve* **2004**, *30*, 182−187.

(21) Pulito, C.; Cristaudo, A.; Porta, C. L.; Zapperi, S.; Blandino, G.; Morrone, A.; Strano, S. Oral mucositis: the hidden side of cancer therapy. *J. Exp. Clin. Cancer Res.* **2020**, *39* (1), 210.

(22) Medrado, A.; Pugliese, L.; Reis, S.; Andrade, Z. Influence of low level laser therapy on wound healing and its biological action upon myofibroblasts. *Lasers Surg. Med.* **2003**, *32*, 239−244.

(23) Gigo-Benato, D.; Geuna, S.; Rochkind, S. Phototherapy for enhancing peripheral nerve repair: a review of the literature. *Muscle Nerve* **2005**, *31*, 694−701.

(24) Anders, J.; Geuna, S.; Rochkind, S. Phototherapy promotes regeneration and functional recovery of injured peripheral nerve. *Neurol. Res.* **2004**, *26*, 233−239.

(25) Anders, J.; Borke, R.; Woolery, S.; Van de Merwe, W. Low power laser irradiation alters the rate of regeneration of the rat facial nerve. *Lasers Surg. Med.* **1993**, *13*, 72−82.

(26) Chung, H.; Dai, T.; Sharma, S. K.; et al. The Nuts and Bolts of Low-level Laser (Light) Therapy. *Ann. Biomed. Eng.* **2012**, *40*, 516−533.

(27) Delley, B. An All-Electron Numerical Method for Solving the Local Density Functional for Polyatomic Molecules. *J. Chem. Phys.* **1990**, *92* (1), 508−517.

(28) Meksiarun, P.; Andriana, B. B.; Matsuyoshi, H.; Sato, H. Non-invasive Quantitative Analysis of Specific Fat Accumulation in Subcutaneous Adipose Tissues using Raman Spectroscopy. *Sci. Rep.* **2016**, *6* (1), 37068.

(29) Bresson, S.; Marssi, M. E.; Khelifa, B. Raman spectroscopy investigation of various saturated monoacid triglycerides. *Chem. Phys. Lipids* **2005**, *134* (2), 119−129.

(30) O'Connor, R. T.; DuPre, E. F.; Feuge, R. O. The infrared spectra of mono-, di-, and triglycerides. *J. Am. Oil Chem. Soc.* **1955**, *32*, 88−93.